Published in final edited form as:
J Comp Neurol. 2010 June 1; 518(11): 1908–1924. doi:10.1002/cne.22310.

Ultrastructural Localization of High-Affinity Choline Transporter in the Rat Anteroventral Thalamus and Ventral Tegmental Area: Differences in Axon Morphology and Transporter Distribution

Ericka C. Holmstrand[1], **Josephine Asafu-Adjei**[3], **Allan R. Sampson**[3], **Randy D. Blakely**[4], and **Susan R. Sesack**[1,2]

[1]Department of Neuroscience, University of Pittsburgh, Pittsburgh, Pennsylvania 15260 USA

[2]Department of Psychiatry, University of Pittsburgh, Pittsburgh, Pennsylvania 15260 USA

[3]Department of Statistics, University of Pittsburgh, Pittsburgh, Pennsylvania 15260 USA

[4]Department of Pharmacology, School of Medicine, and Center for Molecular Neuroscience, Vanderbilt University, Nashville, Tennessee 37232 USA

Abstract

The high-affinity choline transporter (CHT) is a protein integral to the function of cholinergic neurons in the CNS. We examined the ultrastructural distribution of CHT in axonal arborizations of the mesopontine tegmental cholinergic neurons, a cell group in which CHT expression has yet to be characterized at the electron microscopic level. Using silver-enhanced immunogold detection, we compared the morphological characteristics of CHT-immunoreactive axon varicosities specifically within the anteroventral thalamus (AVN) and the ventral tegmental area (VTA). We found that CHT-immunoreactive axon varicosities in the AVN displayed a smaller cross-sectional area and a lower frequency of synapse formation and dense-cored vesicle content than CHT-labeled profiles in the VTA. We further examined the subcellular distribution of CHT and observed that immunoreactivity for this protein was predominantly localized to synaptic vesicles and minimally to the plasma membrane of axons in both regions. This pattern is consistent with the subcellular distribution of CHT displayed in other cholinergic systems. Axons in the AVN showed significantly higher levels of CHT immunoreactivity than those in the VTA and correspondingly displayed a higher level of membrane CHT labeling. These novel findings have important implications for elucidating regional differences in cholinergic signaling within the thalamic and brainstem targets of the mesopontine cholinergic system.

Keywords

acetylcholine; limbic; dopamine; pedunculopontine tegmentum

The Na+/Cl- dependent high-affinity choline transporter (CHT) supplies substrate for the synthesis of acetylcholine (ACh) in central and peripheral cholinergic neurons (Haga and Noda, 1973; Löffelholz and Klein, 2006; Takashina et al., 2008; Wecker and Dettbarn, 1979; Yamamura and Snyder, 1972,1973). Due to its high affinity for choline, this protein can meet the demand for local ACh synthesis during prolonged activation of cholinergic neurons (Simon et al., 1976; Simon and Kuhar, 1975). Blockade of choline transport leads to subsequent depletion of ACh in brain synaptosomes and at the neuromuscular junction

Corresponding author: Susan R. Sesack, PhD, Department of Neuroscience, University of Pittsburgh, Langley Hall, Room 210, Pittsburgh, PA 15260, 412-624-5158, 412-624-9198 fax, sesack@pitt.edu.

(Bazalakova et al., 2007; Guyenet et al., 1973; Zapata et al., 2000). Expression of the transporter is therefore necessary to successful cholinergic transmission and ultimately to survival in mammals (Ferguson et al., 2004).

The regional and cellular expression of CHT mRNA and the localization of CHT protein closely match that of other selective markers of cholinergic phenotype in the rodent and primate nervous system (Ferguson et al., 2003; Kus et al., 2003; Misawa et al., 2001). Nevertheless, the transcription and translation of CHT are dissociable from those of the synthetic enzyme, choline acetyltransferase (ChAT) and the vesicular acetylcholine transporter (VAChT) (Eiden, 1998; Erickson et al., 1994; Lecomte et al., 2005). Furthermore, CHT shows a different expression profile from these other markers during development (Lecomte et al., 2005), following injury (Oshima et al., 2004), and in some pathological conditions (Slotkin et al., 1994; Slotkin et al., 1990).

At the ultrastructural level, CHT is localized mainly to synaptic vesicles in the cytoplasmic compartment of axon terminals, with only a small proportion associated with the plasma membrane (Ferguson et al., 2003; Nakata et al., 2004). This subcellular localization suggests the existence of a recruitable pool of cytoplasmic transporters, consistent with decades of biochemical research showing that high-affinity choline uptake can be dramatically increased through the rapid insertion of new transporters into the plasma membrane, a process mediated by the fusion of CHT-containing synaptic vesicles with the plasmalemma (Antonelli et al., 1981; Ferguson et al., 2003; Ferguson and Blakely, 2004; Haga and Noda, 1973; Murrin and Kuhar, 1976; Roskoski, 1978; Simon and Kuhar, 1975). Membrane-bound CHT is also internalized through clathrin-dependent endocytosis (Ribeiro et al., 2003). The number of membrane bound transporters is therefore determined by the rates of exo- and endocytosis. Furthermore, the rate of endocytosis can be influenced by the activity of protein kinases and phosphatases in the axon terminal (Breer and Knipper, 1990; Gates et al., 2004; Vogelsberg et al., 1997). It therefore seems likely that external signaling events in the vicinity of cholinergic terminals could potentially influence the number of active transporters in the plasma membrane, independent of any action on the rate of acetylcholine release (Breer and Knipper, 1990).

Functional investigations of high-affinity choline uptake in synaptosomes have focused largely on striatal, hippocampal, and cortical tissues. Both the basal rate of choline uptake and modulation of high-affinity choline uptake have been shown to differ between striatal and cortical tissue (Stanton and Johnson, 1987; Wecker and Dettbarn, 1979). This is not surprising given that the cholinergic innervation of the striatum and cortex arise from separate systems. The characteristics of high-affinity choline uptake have not been described for the projections of the brainstem pedunculopontine (PPT) and laterodorsal tegmental (LDT) cholinergic neurons; therefore, it is not known whether the low level of membrane incorporation of CHT is a property of this system as well.

PPT and LDT cholinergic cells provide ascending modulation to a variety of subcortical structures. These neurons are the predominant source of ACh to the thalamus (Hallanger and Wainer, 1988; Sofroniew et al., 1985), and the midbrain ventral tegmental area (VTA) (Gonzalo-Ruiz et al., 1995; Gould et al., 1989). They also project to the basal forebrain cholinergic system (Losier and Semba, 1993), and thus can theoretically influence signaling in a diverse and large group of forebrain structures. It has been suggested that PPT/LDT cholinergic neurons modulate forebrain processing of environmental stimuli, thus facilitating externally directed behavioral responses (Kobayashi and Isa, 2002).

We wished to examine the ultrastructural distribution of CHT protein in the projections of cholinergic PPT/LDT neurons in intact animals. We chose to examine the terminal fields of

these neurons in the VTA because of their demonstrated role in general motivational processes (Ikemoto and Panksepp, 1996; Pan and Hyland, 2005) and their relevance to nicotine addiction in particular (Corrigall et al., 2002; Lança et al., 2000; Laviolette and van der Kooy, 2003; Pidoplichko et al., 2004). For comparison, we examined cholinergic terminals in the anteroventral nuclei of the thalamus (AVN) for two reasons. First, the cholinergic innervation of this particular thalamic nucleus is relatively dense (Heckers et al., 1992; Holmstrand et al., 2006; Sofroniew et al., 1985) and probably arises exclusively from the brainstem cholinergic system (Gonzalo-Ruiz et al., 1995; Shibata, 1992), at least in the rat (see (Parent et al., 1988)). Secondly, the AVN is an important component of the limbic system and so is linked functionally with the VTA, even though there are no direct connections between the two regions (Geisler and Zahm, 2005; Shibata, 1992). We examined CHT-containing axonal profiles in these nuclei at the ultrastructural level and compared the morphology, synaptology, and both the overall density of CHT immunogold reactivity and the specific membrane density of CHT in cholinergic axons innervating these regions. Preliminary accounts of this investigation were previously reported in abstract form (Holmstrand et al., 2006,2008).

Materials and Methods

Subjects

All animal procedures were carried out with approval from the Institutional Animal Care and Use Committee at the University of Pittsburgh. Male Sprague-Dawley rats (Hilltop Lab Animals, Inc., Scottdale, PA) weighing 300–400 g were deeply anesthetized with sodium pentobarbital (60 mg/kg i.p.) and pretreated for 15 minutes with sodium diethyldithiocarbamate (DEDTC, Spectrum Chemical Corp., Gardena, CA; 1 mg/kg i.p.) to prevent silver enhancement of endogenous zinc ions in axon terminals (Veznedaroglu and Milner, 1992). A cohort of paired animals were then perfused using a transcardial approach with 50 mL of heparinized saline (1000 U/mL), followed by 500 mL of 3% paraformaldehyde and 0.15% glutaraldehyde in 0.1 M phosphate buffer, pH 7.4 (PB). The brains were removed and cut in the coronal plane to yield 3–4 mm thick blocks. Tissue was then post-fixed overnight in the same fixative at 4°C. Brains were sectioned through the anterior thalamus and the midbrain to a thickness of 50 μm and collected in PB. Sections were treated with 1% sodium borohydride in PB for 30 minutes and rinsed extensively.

Immunohistochemistry

Sections were labeled by immunoperoxidase or immunogold-silver using a polyclonal antibody raised in rabbit against the C-terminus 15 amino acid sequence that is conserved in the human, mouse and rat CHT protein. Several lines of evidence support the specificity of this antibody (Ferguson et al., 2003). The antiserum labels a band of the predicted molecular weight for CHT by Western blot analysis of mouse whole tissue or brain synaptosomes and from PC12 cells transfected with human CHT. This immunoreactive band is absent from kidney and from PC12 cells transfected with empty vector. Immunohistochemical labeling with the polyclonal rabbit antibody conforms to the expected distribution of cholinergic neurons and fibers throughout the mouse and rat brain and at the neuromuscular junction, and is co-localized with other markers of cholinergic phenotype but not other transmitters. Pre-adsorption with the immunizing peptide abolishes this labeling (Ferguson et al., 2003). Finally, immunolabeling is absent from CHT −/− mice (Ferguson and Blakely, 2004).

Sections for immunoperoxidase visualization of CHT were rinsed in 0.1 M Tris-buffered saline, pH 7.6 (TBS) and incubated for 30 minutes in a blocking solution containing 1% bovine serum albumin (BSA), 5% normal donkey serum (NDS, Jackson Immunoresearch Laboratories, Inc., West Grove, PA), and Triton X-100 (Sigma, St. Louis, MO) at 0.2% or

0.04% for light or electron microscopy, respectively. Sections were then transferred to blocking solution containing the polyclonal rabbit anti-CHT at 1:1000 and incubated overnight at 4°C. After rinsing, sections were incubated for 30 minutes in biotinylated donkey anti-rabbit IgG (Jackson Immunoresearch) diluted at 1:400 in blocking solution. Excess secondary antibody was removed with several rinses in TBS, and sections were incubated in ABC solution (Vectastain kit, Vector Laboratories, Burlingame, CA) for 30 minutes. Peroxidase product was developed by incubation in 0.022% diaminobenzidine (Sigma) and 0.003% hydrogen peroxide for 3 minutes. Sections for light microscopy were rinsed extensively in TBS and 0.01 M phosphate buffered saline prior to mounting on Superfrost microscope slides (Fisher Scientific, Pittsburgh, PA). After drying, slides were dehydrated through a series of increasing ethanol concentrations, defatted in xylene, and coverslipped with Cytoseal-60 mounting medium (Richard Allen Scientific, Kalamazoo, MI). Immunoperoxidase labeled sections for electron microscopy were prepared as detailed below.

Sections for pre-embedding gold-silver immunostaining were treated according to the recommended protocol included with the Aurion RGent SEM kit (Electron Microscopy Sciences, Hatfield, PA). Sections were rinsed in 0.02 M phosphate buffered saline, pH 7.4 (PBS) and permeabilized in 0.05% Triton X-100 for 10 minutes. Non-specific antigenic sites were blocked by a 30 minute incubation in PBS containing 5% BSA, 5% NDS, and 0.1% fish gelatin (GE Healthcare Life Sciences, Waukesha, WI). Sections were then rinsed in an incubation buffer containing 0.2% acetylated BSA (Aurion BSAc, Electron Microscopy Sciences) and incubated overnight at 4°C in incubation buffer containing primary antibody (rabbit anti-CHT, 1:1000). Sections were rinsed extensively in incubation buffer and placed in vials containing secondary antibody (Aurion donkey anti-rabbit 0.8 nm gold conjugate, 1:50, Electron Microscopy Sciences) and 5% NDS in the same buffer. Secondary antibody binding occurred overnight at 4°C. After rinsing in incubation buffer and PBS, antibody complexes were fixed by incubation for 10 minutes in 2% glutaraldehyde in PBS. Following several rinses in PBS, gold particles were silver-enhanced using the Aurion RGENT SEM kit, according to the manufacturer's instructions and using the optional enhancement conditioning solution (Aurion ECS, Electron Microscopy Sciences). Silver enhancement proceeded from 45–75 minutes and was terminated by several rinses in ECS, followed by 0.1 M PB.

Tissue preparation for light and electron microscopy

Brightfield micrographs were captured on an Olympus BX-51 microscope (Olympus America Inc., Center Valley, PA) equipped with a CCD camera (Hamamatsu, Bridgewater, NJ). Acquired images were imported into Adobe Photoshop (Adobe Systems Incorporated, San Jose, CA) and modified to match brightness and contrast.

Immunoperoxidase and immunogold-silver reacted tissue was processed for electron microscopy by incubation in 2% osmium tetroxide in 0.1 M PB for 1 hour, dehydrated through a series of increasing ethanol concentrations, treated with propylene oxide, and infiltrated with an epoxy resin (EMBed-812, Electron Microscopy Sciences). Sections were then flat-embedded between sheets of commercial plastic (Aclar, Electron Microscopy Sciences). Ultrathin (60–70 nm) sections were cut through the regions of interest on a Leica Ultracut ultramicrotome (Leica Microsystems, Bannockburn, IL) and mounted on either copper mesh grids or carbon coated copper slot grids (Electron Microscopy Sciences). Sections were then counterstained with 5% uranyl acetate and lead citrate and examined on a transmission electron microscope (Morgagni, FEI Company, Hillsboro, Oregon) equipped with a CCD camera (Advanced Microscopy Techniques, Danvers, MA). Digital micrographs of labeled axonal profiles were captured at 14,000 – 28,000x magnification and adjusted for exposure and contrast in Adobe Photoshop.

Image analysis

In cholinergic projections to the cortex, it has been shown that the synaptic incidence extrapolated from single section observations is equal to the rate of synapse formation obtained from the analysis of serial ultrathin sections (Umbriaco et al., 1994). However, this relationship has not yet been established for the projections of the PPT/LDT cholinergic cells. We therefore evaluated the rate of synapse formation observed in serial section data and compared this to an extrapolated synaptic incidence calculated from data obtained only from single sections.

For each rat, two vibratome sections were examined through each region. For most CHT immunolabeled profiles, we were able to obtain a series of micrographs from adjacent ultrathin sections, and we used these profiles to determine if each displayed a synaptic specialization (n = 637, Data set #1, Table 1). We also used this first data set to determine whether each CHT labeled profile contained at least one dense-cored vesicle or none.

To further analyze the extent of synapse formation, we utilized a second data set of single sections through CHT immunoreactive profiles from 3 of the 6 animals (n = 410, Data set #2, Table 1) and applied a well-accepted method for post hoc size correction to generate an extrapolated synaptic incidence (Beaudet and Sotelo, 1981). By comparing the values obtained from the serial sections with that extrapolated from single section analysis, we could determine if this extrapolation method can accurately estimate synaptic incidence in these brain regions. More specifically, we recorded the minimum diameter (D), and length of the synaptic junction (d) for each of these profiles. We also measured the thickness of our sections (w) using the minimal fold method (Small, 1968). We computed the means of these measurements for each region, and applied the following equation:

$$P=(d/D)^{*}(2/\pi)+(w/D);$$

where P is the probability of observing a synapse in a single section through an axonal profile if all profiles form one synapse (Beaudet and Sotelo, 1981). In other words, P^{*}(*true synaptic incidence*) = *single-section synaptic incidence*. We therefore divided the rate of synapse formation we observed in our single section sample by this probability (*P*) to generate the extrapolated synaptic incidence.

For the analysis of CHT immunogold localization, we used a third data set consisting of single sections through each profile from both Data sets #1 and #2 (n = 1047, Data set #3, Table 1). To avoid bias in the selection of a single image through the serial micrographs from Data set #1, we chose the image that was photographed first, regardless of its position within the series. In this case, we assumed that the first encounter with a profile constituted a random event.

Using a commercial image analysis software program (SimplePCi, Hamamatsu), we measured immunoreactive profiles and recorded the number of gold particles in the cytoplasm and associated with the plasma membrane. From these data, we derived the following measurements: (1) profile area, 2) profile perimeter, 3) total gold density of CHT immunogold particles, defined as the total number of gold particles per unit profile area, and 4) membrane density of CHT immunogold particles, defined as the number of membrane associated gold particles per unit profile perimeter. Membrane gold particles were defined as those immediately in contact with the plasmalemma or separated by no more than 20 nm, based on estimates of gold particle and immunoglobulin size (Mathiisen et al., 2005).

Silver-enhanced gold particles were observed at high density in axonal profiles that clearly contained synaptic vesicles. The presence of a lower density of gold-silver particles in some dendrites suggested a certain degree of background staining, which varied between animals. Therefore, when there was any concern regarding specific gold labeling in axons, these profiles were followed in a short series of adjacent sections. Profiles that contained fewer than 10 gold particles per square micron were excluded from our sample unless consistent immunolabeling was observed in at least 3 serial micrographs. Non-specific background labeling was similar in the two regions, averaging 1.6 ± 1.3 gold particles per μm^2 in the AVN vs. 1.7 ± 1.4 gold particles per μm^2 in the VTA. Specific gold-silver labeling in the final data set was determined to be at least 2.5 times above background levels, with the majority of profiles well beyond this minimum level.

Statistical analysis

Serial micrographs from the first data set (Table 1) were examined for the *presence of synaptic specializations and dense-cored vesicles*. The probabilities of synapse presence and dense-cored vesicle presence were modeled using generalized linear mixed models based on the Bernoulli distribution, with the logit as the link function. Brain region was treated as a fixed effect. Animal pair was also treated as a fixed effect to account for the fact that animal tissue was processed in pairs. To account for the correlation among observations within an animal and among observations within each Vibratome section, animal and section nested in animal were treated as independent normally distributed random effects.

The remaining dependent measures were analyzed from the third data set of all labeled profiles (Table 1). A linear mixed model was used to model the *profile area of CHT-immunoreactive structures*, with brain region and animal pair treated as fixed effects. To account for the correlation among observations within an animal and among observations within each Vibratome section, animal and section nested in animal were treated as independent normally distributed random effects.

A generalized linear mixed model, based on a Poisson distribution, was used to model *total gold density of CHT immunogold positive profiles*, with the log as the link function and the natural logarithm of profile area as an offset variable. Brain region and animal pair were treated as fixed effects. To account for the correlation among observations within an animal and among observations within each Vibratome section, animal and section nested in animal were treated as independent normally distributed random effects.

Membrane density of CHT immunogold positive profiles was modeled in a manner similar to that of *total gold density of CHT immunogold positive profiles*. The only difference arose from the fact that the model for membrane density used the natural logarithm of profile perimeter as an offset variable and included total gold density and the interaction between brain region and total gold density as fixed effects, in addition to brain region and animal pair.

The analysis of profile area was implemented in SAS PROC MIXED (Version 9.2, SAS Institute Inc., Cary, NC), while all other analyses were implemented in SAS PROC GLIMMIX. The Kenward-Roger degrees of freedom method was used in each analysis. When testing for the significance of fixed effects in a mixed model, the Kenward-Roger method is generally recommended to approximate the denominator degrees of freedom in subsequent F tests (Littell et al., 2006). This method corrects for the fact that the estimated variability of the fixed effects parameter estimates tends, on average, to be lower than the actual variability of these estimates.

All statistical tests were conducted at the 0.05 significance level.

Results

Light microscopic detection of CHT

Immunoperoxidase staining was used to examine the distribution of CHT in the AVN and VTA (Fig. 1). The AVN division of the thalamus contained dense puncta immunoreactive for CHT that were suggestive of axon varicosities. Such profiles were notably absent from the adjacent anterodorsal thalamic nucleus (Fig. 1A). In the VTA, similar axon-like immunoreactive puncta were observed, although the innervation appeared to be less dense (Fig. 1B).

Ultrastructural detection of CHT

Immunoperoxidase labeling for CHT was observed mainly in unmyelinated axonal profiles in the AVN and VTA (Fig 2). By qualitative estimation of both light and electron micrographs, it appeared that the AVN contained a higher density of CHT-labeled profiles (Fig. 1, inserts; Fig. 2); however, this was not quantified further. In the VTA, occasional myelinated axons were also found to contain CHT. The efferent fibers of the oculomotor nerve pass through the VTA without synapsing, and given that these are cholinergic premotor axons, we restricted our examination to only the unmyelinated profiles likely to represent brainstem cholinergic axons. Immunogold-silver labeling for CHT was also localized primarily to unmyelinated axonal profiles in the AVN and VTA (Fig 3). With either staining method, CHT-labeled axon varicosities in both regions formed axodendritic synapses with either symmetric or asymmetric morphology and contained mainly small-clear and occasional dense-cored vesicles (Figs. 2,3). These morphological features were more easily visualized with the immunogold-silver method, and this approach was therefore used to investigate regional differences in the frequency of observation of synaptic specializations and dense-cored vesicles (see below). By either immunoperoxidase or immunogold labeling methods, CHT-containing axons in the AVN appeared to be smaller and more densely labeled than profiles in the VTA. These apparent differences were also compared quantitatively using immunogold-silver labeling for CHT.

Morphological features of CHT-labeled axon varicosities in the AVN and VTA

For the more exhaustive approach of counting synapses in serial sections, we included only profiles for which 3 or more serial micrographs were available to examine. This subset of CHT-labeled profiles was also used for statistical comparison between the AVN and VTA. The majority of this data came from 5 of the 6 rats (Data set #1, Table 1); sections from animal 2 were collected only on mesh grids and yielded few sets of serial micrographs. In the AVN, 333 CHT-immunoreactive axon varicosities were examined in serial ultrathin sections, and of these, 120 (36%) formed synaptic specializations of the symmetric or asymmetric type. In the VTA, 304 CHT-labeled profiles were analyzed in serial, and 144 of these (47%) were synaptic. There was a significant effect of region on the synaptic incidence of the profiles examined ($t_{(633)}= -2.69$, $p = 0.0074$), indicating that CHT axons in the VTA were more commonly observed to form synapses than those in the AVN. There was no significant effect of animal pair. Furthermore, there were no apparent differences across region in the extent to which CHT-labeled profiles formed symmetric (33% in the AVN versus 34% in the VTA) or asymmetric (60% in the AVN versus 54% in the VTA) synapse types; the remaining synapses had indeterminate morphology.

From single sections (Data set #2, Table 1), we observed 51 synapses from a total of 205 CHT-labeled varicosities (25%) in the AVN. In the VTA, we observed 60 synapses from a total of 205 CHT-labeled profiles examined (29%). These profiles had a mean diameter of 0.38 μm (AVN) and 0.58 μm (VTA), with a mean synapse length of 0.32 μm (AVN) and 0.47 μm (VTA). The mean section thickness in these micrographs was 65 nm (AVN) and 69

nm (VTA). Using the equation described in the methods, we obtained an extrapolated synaptic incidence of 35% in the AVN, compared to 36% observed in our serial sections. For the VTA, the extrapolated synaptic incidence was 47%, identical to the rate observed in our serial sections. The close agreement of the extrapolated synaptic incidence with results obtained from serial ultrathin section analysis suggests that extrapolation from single sections is an appropriate method for application to the brainstem cholinergic projection system, and may be used in place of the more labor-intensive serial examination.

CHT-positive varicosities were also analyzed in serial sections to determine whether dense-cored vesicles were present. In the AVN, 13% (44/333) of CHT-labeled profiles contained at least one dense-cored vesicle, compared to 29% (87/304) in the VTA. This regional difference was also statistically significant ($t_{(17.5)}= -2.58$, $p = 0.0191$), confirming that dense-cored vesicles were more commonly observed in the VTA CHT-positive population. There was no significant effect of animal pair.

Size of CHT-labeled axon terminals in the AVN and VTA

To quantify possible regional differences in the size and immunolabeling density of CHT-positive profiles, a larger data set was utilized in which profiles were collected from both serial and single section analyses (Data set #3, Table 1). For the AVN, 538 CHT-positive axon varicosities were measured, and their mean size was 0.41 μm^2 (± 0.13 SD). In the VTA, 509 profiles had a mean size of 0.63 μm^2 (± 0.12 SD). Figure 4 shows the distribution of observed profile areas and illustrates that similar ranges of areas were observed for both regions and that the distributions were overlapping. However, a large proportion of AVN profiles had small areas (> 90% in the first three bins), whereas VTA profiles were more likely to be of moderate area, as evidenced by the rightward shift of the VTA distribution compared to that of the AVN (Fig. 4A). Statistically, there was a significant regional difference in profile area ($t_{(20.6)} = -4.18$; $p = 0.0004$), indicating that the population of CHT-positive varicosities in the AVN is on average smaller than that in the VTA. There was also a significant effect of animal pair ($F_{(2, 20.6)} = 6.49$; $p = 0.007$). The reason for this is not clear, but it might reflect the fact that animals within pairs were more likely to be the same age and weight and might even have been litter mates. Alternatively, the significant effect of animal pair might be due to differences in tissue shrinkage during the fixation, dehydration, and/or plastic embedding processes that would be expected to occur, as animal pairs were processed at different times.

Total gold and membrane gold densities of CHT-labeled axon terminals in the AVN and VTA

CHT-labeled varicosities in the AVN appeared to contain more total gold-silver particles than those in the VTA, although a considerable range was also evident (Figs. 3, 5). In the AVN, CHT-positive axon varicosities had a mean total gold density of 43.5 (± 17.0 SD) gold particles per unit area versus a density of 22.8 (± 4.4 SD) in the VTA. As shown in Figure 6A,B, this difference reflects a larger proportion of profiles with low total gold in the VTA as compared to the AVN. The total gold density of CHT-labeled axonal profiles was significantly different between the AVN and VTA populations ($F_{(1, 20)} = 18.89$, $p = 0.0003$). There was also a significant effect of animal pair ($F_{(2, 20)} = 4.45$, $p = 0.0252$), indicating that total gold density was more similar within than across pairs. This is not surprising given that tissue from paired cohorts were processed at separate times using different batches of immunoreagents.

The greater density of total gold labeling might be expected to raise the probability of gold-silver particles contacting the plasma membrane (compare for example, Fig. 5A and 5D). Therefore the set of all CHT-labeled profiles was also analyzed for membrane gold density,

which had mean values of 1.05 (± 0.42 SD) and 0.55 (± 0.09 SD) gold particles per unit perimeter in the AVN and VTA, respectively. As shown in Figure 6 C,D, this apparent difference reflects a larger proportion of profiles with high membrane gold densities in the AVN versus the VTA. The difference in membrane gold density was significant between regions ($F_{(1,25.14)} = 24.32$, $p < 0.0001$); the effect of animal pair was not significant. As expected, total gold density also had a significant effect on membrane gold density ($F_{(1, 1041)} = 684.00$, $p < 0.0001$). However, there was also a significant interaction effect of region and total gold density on the membrane gold density ($F_{(1, 1041)} = 21.94$, $p < 0.0001$), indicating that although membrane gold density was dependent on total gold density in both regions, the relationship between these variables differed significantly between regions. In other words, total gold density drove membrane gold density in a region-specific manner.

Discussion

This study represents the first ultrastructural investigation of the distribution of CHT in the rat thalamus and midbrain as representative target areas of the brainstem mesopontine cholinergic system. The morphology and synaptology of the axons displaying CHT immunoreactivity in both regions were relatively well matched to profiles identified by other markers of cholinergic projections in the published literature. Nevertheless, direct comparison of CHT immunolabeled boutons in the rat AVN versus the VTA revealed some important differences, both in the morphological characteristics of these axon varicosities, and in the density and localization of the transporter. Labeled axons in the AVN were smaller and less frequently formed synaptic specializations with neuronal elements than those in the VTA. AVN profiles were also less frequently observed to contain dense-cored vesicles. Finally, AVN varicosities contained more total CHT immunogold particles than their VTA counterparts and showed a higher density of transporters associated with the plasma membrane.

Limitations of the methods

The principal limitation of immunoelectron microscopy is the potential for false negative results based on restricted penetration of immunoreagents. The efficiency of the preembedding immunogold-silver method in particular is limited by incomplete penetration of gold-conjugated secondary antibodies, and the need to minimize exposure to detergents that degrade phospholipid membranes. To reduce false negatives, we therefore examined tissue from only the first few microns of each section. We also used a stringent but consistent inclusion criterion to avoid false positives (see Materials and Methods). Therefore, we acknowledge that our sampling may have excluded some cholinergic axons that express low levels of CHT. As profiles in the VTA generally displayed a lower level of staining overall, this may have resulted in a more restricted sample population in this region. Nevertheless, the analysis involved thalamic and midbrain sections from the same animals exposed to the same batches of immunoreagents and subjected to the same sampling scheme. Moreover, the range of observed values overlapped considerably for both regions. Hence, the reported findings are likely to reflect true regional differences.

An additional limitation of the preembedding immunogold-silver method of antigen detection is the relative inefficiency of labeling membrane proteins in the synapse (Baude et al., 1995; Bernard et al., 1997). While this method localizes extrasynaptic membrane proteins well, the density of the synaptic space and associated structures reduces the ability of antibodies to gain full access to all available epitopes, hence increasing the likelihood of false negative staining specifically at this site. To determine with certainty the presence of transporters within synaptic membranes, post-embedding methods must be employed. However, we found that the antigenicity of CHT was not preserved following plastic embedding, thus preventing application of this more sensitive method. Therefore, our results

concerning differences in the membrane density of CHT are applicable only to the extrasynaptic portions of the axonal membrane.

Finally, we must acknowledge that the low level of immunogold-reactivity associated with the plasma membrane may reflect a preferential association of the primary antibody with cytoplasmic transporters and reduced epitope recognition of membrane-bound transporters. This could occur if association with the phospholipid membrane induced allostearic changes in the structure of the intracellular tail of CHT, or if the tail structure is otherwise different between the two states (e.g. through phosphorylation or interaction with scaffolding proteins). It should be noted that our sample included axonal profiles from each region that showed greater numbers of membrane transporters than cytoplasmic transporters, demonstrating that the heavily cytoplasmic staining is not artifactual. Nonetheless, we cannot exclude the possibility of a physical bias in immunoreactivity.

Population characteristics of AVN and VTA CHT-positive varicosities

Our sample of CHT-positive boutons most likely represents cholinergic axons arising from the ascending projections of the tegmental cholinergic cell groups. To date, CHT expression in the brain has only been reported in cholinergic neurons (Okuda and Haga, 2003), and the pattern of immunoreactivity closely matches that of vAChT and ChAT (Kus et al., 2003; Misawa et al., 2001). Hence, immunoreactivity for CHT serves as an exclusive marker of cholinergic axons. Furthermore, the AVN and VTA appear to receive cholinergic innervation predominantly from neurons in the brainstem mesopontine tegmentum (Gonzalo-Ruiz et al., 1995; Jones and Beaudet, 1987; Sofroniew et al., 1985; Yeomans, 1995). Although a minor projection from basal forebrain cholinergic cells to the AVN has been proposed (Hallanger et al., 1987; Parent et al., 1988), the majority of the cholinergic innervation to this region is believed to arise from the brainstem (Heckers et al., 1992). Furthermore, the AVN is not immunoreactive for the nerve growth factor (NGF) receptor (Yan and Johnson, 1989), a selective marker of basal forebrain cholinergic axons (Woolf et al., 1989). The VTA is innervated by some neurons in the basal forebrain (Geisler and Zahm, 2005; Grove, 1988; Tomimoto et al., 1987), but these have never been demonstrated to be cholinergic. Moreover, the VTA regions that receive these projections are also devoid of NGF immunoreactivity (Yan and Johnson, 1989), and other authors have asserted that the PPT and LDT represent the sole source of cholinergic afferents to the VTA (Yeomans et al., 1993).

The morphology and synaptology of CHT-labeled axons in the thalamus and midbrain closely match previous descriptions of cholinergic boutons within these regions, including the relatively small size, content of small clear vesicles, and predominant formation of axodendritic synapses (Garzón et al., 1999; Hallanger et al., 1990; Oda et al., 2003; Omelchenko and Sesack, 2006). The presence of numerous dense-cored vesicles in these varicosities appears not to have been reported previously, most likely due to the masking effect of heavy immunoperoxidase product in prior studies.

Our sample of CHT-labeled varicosities did display some distinct differences in synaptology as compared to cholinergic populations described in the published literature. For example, Oda et al. reported a higher incidence of vAChT-labeled axons forming synapses in the AVN (~60% versus 35–36% in the present study). Moreover, both vAChT and ChAT-labeled axons have been reported to synapse onto cell bodies in this region (Hallanger et al., 1990; Oda et al., 2003), which we did not observe. In the VTA, the frequency of synapses reported here is better matched to previous estimates (~ 50% versus the present 47%) (Garzón et al., 1999; Omelchenko and Sesack, 2006). Nevertheless, we again did not observe any CHT-containing axosomatic synapses in the VTA, despite prior reports of these

synapses using other markers of cholinergic axons (Garzón et al., 1999; Omelchenko and Sesack, 2006).

The reasons for these discrepancies are not immediately clear, although differences in the sampling strategies used across studies are likely to contribute. For example, studies focused on identifying the post-synaptic targets of cholinergic axons may have been biased towards varicosities that were in direct apposition to other neuronal elements and therefore more likely to be observed making synapses (Oda et al., 2003). Our sample included all axonal profiles that contained synaptic vesicles and CHT immunoreactivity in excess of our inclusion threshold, leading us to examine both synapsing and non-synapsing varicosities. Alternatively, both the lower synaptic frequency of CHT-positive profiles in the AVN observed in our study and our failure to detect axosomatic synapses in both regions could indicate that CHT-labeled boutons constitute a subset of all cholinergic varicosities in the AVN and VTA. Additional studies using dual immunolabeling methods for CHT and VAChT are required to address this possibility.

Interestingly, the extrapolated synaptic incidence of cholinergic boutons in the AVN in this study (35%) is similar to that that observed in other thalamic nuclei receiving PPT/LDT cholinergic projections, including the reticular nucleus of the thalamus (33%) and the dorsolateral geniculate nucleus (39%), but stands in contrast to the cholinergic innervation of the parafascicular nucleus of the thalamus, where the incidence is reportedly 100% (Parent and Descarries, 2008). As noted by those authors, this contrast suggests that the formation of synapses may be determined by the functional role(s) played by acetylcholine in each distinct region.

Differences between AVN and VTA CHT-labeled profiles

Variable rates of ACh turnover have been reported between the striatum and cerebral cortex (Wecker and Dettbarn, 1979), indicating a lack of uniformity in functional measures across different cholinergic cell groups in the CNS. Whether this functional variability in ACh transmission reflects structural differences in these axons or their content of CHT remains to be addressed. Still, it is tempting to speculate that the differences we observed in morphology, synaptology, and CHT distribution between cholinergic axons in the AVN and VTA have functional correlates. According to a general scaling principle (Pierce and Lewin, 1994), axon terminal size is positively correlated with activity. It is important to note that this principle has been demonstrated only for amino acid transmitter-containing axons (Lisman and Harris, 1993; Pierce and Lewin, 1994) and has not yet been investigated for cholinergic systems. Still, CHT-positive varicosities in the VTA might be more active and release greater amounts of ACh based on their larger size and higher apparent rate of synapse formation. Alternatively, the higher total content and greater membrane distribution of CHT in AVN profiles suggests an overall higher demand for ACh synthesis that necessitates steady replenishment of choline. It is difficult to reconcile these seemingly paradoxical observations, and neurochemical studies are needed to specifically test for differences in ACh transmission between the thalamus and midbrain.

In addition to possible differences in overall activity level, it could be that the pattern of ACh release also differs between these areas and that this results in distinct demands for choline uptake. Different activity patterns have been recorded for presumed cholinergic neurons in the mesopontine tegmentum, including cells whose firing varies across sleep-wake states, as well as neurons with state-independent activity (Datta and Siwek, 2002; Koyama et al., 1994). If cells with phasic patterns of ACh release innervate the VTA, then their axonal stores of transmitter could be replenished during quiescent periods using a relatively small number of membrane-associated transporters. Conversely, AVN cholinergic axons might be subjected to tonic activity patterns that require greater continuous reuptake

of choline and therefore a higher level of membrane CHT. In this regard, it is interesting to note that increased membrane CHT has been reported in the cerebral cortex during sustained attention tasks that require tonically accelerated ACh transmission (Apparsundaram et al., 2005).

The fact that many CHT-labeled boutons in both the thalamus and midbrain failed to display evident synaptic specializations suggests that ACh released from brainstem cholinergic cells may be acting on extrasynaptic targets through volume transmission, as already suggested for forebrain cholinergic systems (Descarries et al., 1997). The lower apparent rate of synapse formation in the AVN as compared to the VTA further suggests that volume transmission may play a more important role in the former structure. Nevertheless, there is evidence consistent with extrasynaptic ACh transmission in both regions. For example, the AVN is likely to be the source of ACh for the adjacent anterodorsal thalamic nucleus that expresses cholinergic receptors (Sikes and Vogt, 1987; Vogt et al., 1992) but lacks direct cholinergic input (Levey et al., 1987; Oda et al., 2003). For the VTA, diffuse ACh transmission has been suggested based on the localization of α7 nicotinic receptors on glutamate axon terminals (Jones and Wonnacott, 2004) and the absence of axo-axonic synapses in this region.

Finally, the higher dense-cored vesicle content observed for VTA versus AVN cholinergic boutons suggests that peptide co-transmission may play a larger role in the modulation of VTA neurons. Cholinergic cells in the mesopontine tegmentum have been demonstrated to synthesize and release substance P (Sutin and Jacobowitz, 1990; Vincent et al., 1983) and these neurons may utilize other peptide co-transmitters as well (Crawley et al., 1985; Standaert et al., 1986).

Functional significance

It is interesting to note that, while the AVN and VTA have no direct connections between them (Beckstead et al., 1979; Simon et al., 1979), and even project to distinctly separate cortical and subcortical regions (Bentivoglio et al., 1993), both nuclei have been implicated in cue-driven behavior (Gabriel et al., 1980; Pan and Hyland, 2005). The AVN is best recognized for its contribution to spatial memory (Warburton and Aggleton, 1999) but also partially mediates conditioned avoidance responses (Gabriel et al., 1980; Sparenborg and Gabriel, 1992). In contrast, the VTA plays a crucial role in conveying reward prediction to forebrain circuits that determine behavioral output (Redgrave et al., 2008; Schultz, 2007). The cholinergic input to the VTA is especially necessary for both novel and conditioned cue-driven responses of VTA dopamine neurons (Ikemoto and Panksepp, 1996; Pan and Hyland, 2005). Hence, it seems likely that both the AVN and VTA must receive information about external cues that can guide behavior. This information might be transmitted by cholinergic neurons in the PPT and LDT, as these neurons are responsive to sensory input (Grant and Highfield, 1991; Pan and Hyland, 2005). It is therefore tempting to speculate that environmental stimuli could influence divergent parts of the limbic system through collateral projections from the cholinergic brainstem. Collateralized projections of cholinergic neurons to thalamic nuclei and other regions have been documented (Bolton et al., 1993; Jourdain et al., 1989; Oakman et al., 1999; Semba et al., 1990), although to date the possible existence of such projections to the VTA and AVN has not been explored. Alternatively, such information may be relayed by the non-cholinergic neurons in these regions, or through separate populations of cells.

If the projections to the AVN and VTA are ultimately shown to arise from a common brainstem cell population, then the regional differences observed here in CHT-labeled axons would argue for local factors being the main determinants of bouton morphology and CHT distribution. This supposition is supported by recent evidence that the cholinergic

innervation of several thalamic nuclei displays striking differences in synaptic incidence, even when this innervation arises from similar sources (Parent and Descarries, 2008). In regard to differences in CHT distribution, CHT localization and function can be influenced by intracellular signaling events triggered by the activity of neurotransmitter receptors on the surface of cholinergic axons (Breer and Knipper, 1990). Increases in high-affinity choline transport can be achieved through activation of protein kinase A or C, and corresponding decreases can be effected by phosphatase 1/2A (Breer and Knipper, 1990; Gates et al., 2004). It is therefore plausible that the heterogeneity of CHT labeling observed in this study reflects differences in the extracellular milieu in the AVN versus the VTA. Our finding of a significant interaction effect of region and total gold density on the membrane gold density of CHT-labeled axonal profiles is consistent with some as yet unidentified factor that is differentially active in these regions. One possibility is that the presence of extracellular dopamine released from somatodendritic compartments in the VTA might decrease the membrane density of CHT in this region. This possibility is supported by *in vivo* data showing that elevated extracellular dopamine levels in the striatum are associated with reductions in high-affinity choline transport, consistent with decreased membrane levels of CHT (Parikh et al., 2006).

Alternatively, the differential expression of the choline-sensitive α7 nicotinic acetylcholine receptor (nAChR) may contribute to the differences in membrane CHT content reported here. In the VTA, activation of presynaptic α7 nAChRs results in the potentiation of glutamate release from excitatory afferents (Jones and Wonnacott, 2004; Schilström et al., 2000), but all forms of cholinergic transmission in the AVN are mediated through non-α7 nAChRs (Guseva et al., 2006; Rasmussen and Perry, 2006). The α7 nAChR is desensitized by extracellular choline (Alkondon and Albuquerque, 2006; Alkondon et al., 1997; Mike et al., 2000; Uteshev et al., 2003). Hence, the membrane content of CHT might be inversely correlated with the availability of α7-mediated modes of cholinergic transmission. In this case, the lower membrane content of CHT in the VTA might be driven by a need to keep extracellular choline levels high, thereby restricting the activation of α7 nAChRs and preventing excessive glutamate excitation.

Although differential regulation of choline transport could be accomplished at a local level, the collective morphological differences observed between the CHT-immunolabeled axons in the AVN and VTA are most easily explained by cholinergic innervations arising from separate populations of neurons in the mesopontine tegmentum. Alternatively, the parent populations of AVN and VTA cholinergic inputs could be partially overlapping subsets of PPT/LDT cholinergic cells. This mixed afferent population could produce a range of axon characteristics that favor smaller varicosities with more dense CHT content in the AVN and the converse characteristics in the VTA. This idea is supported by tract-tracing studies showing input from both PPT and LDT populations to the VTA (Oakman et al., 1995; Omelchenko and Sesack, 2005; Satoh and Fibiger, 1986), but a heavier input from the LDT to the AVN (Shibata, 1992). Tract-tracing studies will be essential for clarifying the nature of these circuits and facilitating a systems-level interpretation of the present findings.

Acknowledgments

NIH grants MH067937 for SRS and HL056693 and MH073159 for RDB.

Literature Cited

Alkondon M, Albuquerque EX. Subtype-specific inhibition of nicotinic acetylcholine receptors by choline: a regulatory pathway. J Pharmacol Exp Ther. 2006; 318:268–275. [PubMed: 16565162]

Alkondon M, Pereira EFR, Cortes WS, Maelicke A, Albuquerque EX. Choline is a selective agonist of α7 nicotinic acetylcholine receptors in the rat brain neurons. Eur J Neurosci. 1997; 9:2734–2742. [PubMed: 9517478]

Antonelli T, Beani L, Bianchi C, Pedata F, Pepeu G. Changes in synaptosomal high affinity choline uptake following electrical stimulation of guinea-pig cortical slices: effect of atropine and physostigmine. Br J Pharmacol. 1981; 74:525–531. [PubMed: 7296161]

Apparsundaram S, Martinez V, Parikh V, Kozak R, Sarter M. Increased capacity and density of choline transporters situated in synaptic membranes of the right medial prefrontal cortex of attentional task-performing rats. J Neurosci. 2005; 25:3851–3856. [PubMed: 15829637]

Baude A, Nusser Z, Molnár E, McIlhinney RA, Somogyi P. High-resolution immunogold localization of AMPA type glutamate receptor subunits at synaptic and non-synaptic sites in rat hippocampus. Neuroscience. 1995; 69:1031–1055. [PubMed: 8848093]

Bazalakova MH, Wright J, Schneble EJ, McDonald MP, Heilman CJ, Levey AI, Blakely RD. Deficits in acetylcholine homeostasis, receptors and behaviors in choline transporter heterozygous mice. Genes Brain Behav. 2007; 6:411–424. [PubMed: 17010154]

Beaudet A, Sotelo C. Synaptic remodeling of serotonin axon terminals in rat agranular cerebellum. Brain Res. 1981; 206:305–329. [PubMed: 7214137]

Beckstead RM, Domesick VB, Nauta WJH. Efferent connections of the substantia nigra and ventral tegmental area in the rat. Brain Res. 1979; 175:191–217. [PubMed: 314832]

Bentivoglio, M.; Kultas-Ilinsky, K.; Ilinsky, I. Limbic thalamus: structure, intrinsic organization, and connections. In: Vogt, BA.; Gabriel, M., editors. Neurobiology of Cingulate Cortex and Limbic Thalamus. Boston: Birkhauser; 1993. p. 71-122.

Bernard V, Somogyi P, Bolam JP. Cellular, subcellular, and subsynaptic distribution of AMPA-type glutamate receptor subunits in the neostriatum of the rat. J Neurosci. 1997; 17:819–833. [PubMed: 8987803]

Bolton RF, Cornwall J, Phillipson OT. Collateral axons of cholinergic pontine neurones projecting to midline, mediodorsal and parafascicular thalamic nuclei in the rat. J Chem Neuroanat. 1993; 6:101–114. [PubMed: 8476540]

Breer H, Knipper M. Regulation of high affinity choline uptake. J Neurobiol. 1990; 21:269–275. [PubMed: 2155301]

Corrigall WA, Coen KM, Zhang J, Adamson LK. Pharmacological manipulations of the pedunculopontine tegmental nucleus in the rat reduce self-administration of both nicotine and cocaine. Psychopharmacology (Berl). 2002; 160:198–205. [PubMed: 11875638]

Crawley JN, Olschowka JA, Diz DI, Jacobowitz DM. Behavioral significance of the coexistence of substance P, corticotropin releasing factor, and acetylcholinesterase in lateral dorsal tegmental neurons projecting to the medial frontal cortex of the rat. Peptides. 1985; 6:891–901. [PubMed: 2417203]

Datta S, Siwek DF. Single cell activity patterns of pedunculopontine tegmentum neurons across the sleep-wake cycle in the freely moving rats. J Neurosci Res. 2002; 70:611–621. [PubMed: 12404515]

Descarries L, Gisiger V, Steriade M. Diffuse transmission by acetylcholine in the CNS. Prog Neurobiol. 1997; 53:603–625. [PubMed: 9421837]

Eiden LE. The cholinergic gene locus. J Neurochem. 1998; 70:2227–2240. [PubMed: 9603187]

Erickson JD, Varoqui H, Schäfer M, Modi W, Diebler MF, Weihe E, Rand J, Eiden LE, Bonner TI, Usdin T. Functional characterization of the mammalian vesicular acetylcholine transporter and its expression from a "cholinergic" gene locus. J Biol Chem. 1994; 269:21929–21932. [PubMed: 8071310]

Ferguson S, Savchenko V, Apparsundaram S, Zwick M, Wright J, Heilman C, Yi H, Levey A, Blakely R. Vesicular localization and activity-dependent trafficking of presynaptic choline transporters. J Neurosci. 2003; 23:9697–9709. [PubMed: 14585997]

Ferguson SM, Bazalakova M, Savchenko V, Tapia JC, Wright J, Blakely RD. Lethal impairment of cholinergic neurotransmission in hemicholinium-3-sensitive choline transporter knockout mice. Proc Natl Acad Sci USA. 2004; 101:8762–8767. [PubMed: 15173594]

Ferguson SM, Blakely RD. The choline transporter resurfaces: new roles for synaptic vesicles? Mol Interv. 2004; 4:22–37. [PubMed: 14993474]

Gabriel M, Foster K, Orona E. Interaction of laminae of the cingulate cortex with the anteroventral thalamus during behavioral learning. Science. 1980; 208:1050–1052. [PubMed: 7375917]

Garzón M, Vaughan RA, Uhl GR, Kuhar MJ, Pickel VM. Cholinergic axon terminals in the ventral tegmental area target a subpopulation of neurons expressing low levels of the dopamine transporter. J Comp Neurol. 1999; 410:197–210. [PubMed: 10414527]

Gates J Jr, Ferguson SM, Blakely RD, Apparsundaram S. Regulation of choline transporter surface expression and phosphorylation by protein kinase C and protein phosphatase 1/2A. J Pharmacol Exp Ther. 2004; 310:536–545. [PubMed: 15064333]

Geisler S, Zahm DS. Afferents of the ventral tegmental area in the rat-anatomical substratum for integrative functions. J Comp Neurol. 2005; 490:270–294. [PubMed: 16082674]

Gonzalo-Ruiz A, Sanz-Anquela MJ, Lieberman AR. Cholinergic projections to the anterior thalamic nuclei in the rat: a combined retrograde tracing and choline acetyl transferase immunohistochemical study. Anat Embryol. 1995; 192:335–349. [PubMed: 8554167]

Gould E, Woolf NJ, Butcher LL. Cholinergic projections to the substantia nigra from the pedunculopontine and laterodorsal tegmental nuclei. Neuroscience. 1989; 28:611–623. [PubMed: 2710334]

Grant SJ, Highfield DA. Extracellular characteristics of putative cholinergic neurons in the rat laterodorsal tegmental nucleus. Brain Res. 1991; 559:64–74. [PubMed: 1782561]

Grove EA. Efferent connections of the substantia innominata in the rat. J Comp Neurol. 1988; 277:347–364. [PubMed: 2461973]

Guseva MV, Hopkins DM, Pauly JR. An autoradiographic analysis of rat brain nicotinic receptor plasticity following dietary choline modification. Pharmacol Biochem Behav. 2006; 84:26–34. [PubMed: 16753203]

Guyenet P, Lefresne P, Rossier J, Beaujouan JC, Glowinski J. Effect of sodium, hemicholinium-3 and antiparkinson drugs on [^{14}C]acetylcholine synthesis and [^{3}H]choline uptake in rat striatal synaptosomes. Brain Res. 1973; 62:523–529. [PubMed: 4148552]

Haga T, Noda H. Choline uptake systems of rat brain synaptosomes. Biochim Biophys Acta. 1973; 291:564–575. [PubMed: 4690869]

Hallanger AE, Levey AI, Lee HJ, Rye DB, Wainer BH. The origins of cholinergic and other subcortical afferents to the thalamus in the rat. J Comp Neurol. 1987; 262:105–124. [PubMed: 2442206]

Hallanger AE, Price SD, Lee HJ, Steininger TL, Wainer BH. Ultrastructure of cholinergic synaptic terminals in the thalamic anteroventral, ventroposterior, and dorsal lateral geniculate nuclei of the rat. J Comp Neurol. 1990; 299:482–492. [PubMed: 2243163]

Hallanger AE, Wainer BH. Ascending projections from the pedunculopontine tegmental nucleus and the adjacent mesopontine tegmentum in the rat. J Comp Neurol. 1988; 274:483–515. [PubMed: 2464621]

Heckers S, Geula C, Mesulam MM. Cholinergic innervation of the human thalamus: dual origin and differential nuclear distribution. J Comp Neurol. 1992; 325:68–82. [PubMed: 1282919]

Holmstrand EC, Sesack SR, Blakely RD. Ultrastructural characterization of the expression of the high-affinity choline transporter in the rat ventral tegmental area. Society for Neuroscience Abstracts 728.6. 2006

Holmstrand EC, Sesack SR, Blakely RD. High affinity choline transporter in the rat ventral tegmental area and anteroventral thalamus: colocalization with the vesicular acetylcholine transporter and subcellular distribution to the plasma membrane. Society for Neuroscience Abstracts 129.2. 2008

Ikemoto S, Panksepp J. Dissociations between appetitive and consummatory responses by pharmacological manipulations of reward-relevant brain regions. Behav Neurosci. 1996; 110:331–345. [PubMed: 8731060]

Jones BE, Beaudet A. Retrograde labeling of neurones in the brain stem following injections of [^{3}H]choline into the forebrain of the rat. Exp Brain Res. 1987; 65:437–448. [PubMed: 3556470]

Jones IW, Wonnacott S. Precise localization of α7 nicotinic acetylcholine receptors on glutamatergic axon terminals in the rat ventral tegmental area. J Neurosci. 2004; 24:11244–11252. [PubMed: 15601930]

Jourdain A, Semba K, Fibiger HC. Basal forebrain and mesopontine tegmental projections to the reticular thalamic nucleus: an axonal collateralization and immunohistochemical study in the rat. Brain Res. 1989; 505:55–65. [PubMed: 2575437]

Kobayashi Y, Isa T. Sensory-motor gating and cognitive control by the brainstem cholinergic system. Neural Netw. 2002; 15:731–741. [PubMed: 12371523]

Koyama Y, Jodo E, Kayama Y. Sensory responsiveness of "broad-spike" neurons in the laterodorsal tegmental nucleus, locus coeruleus and dorsal raphe of awake rats: implications for cholinergic and monoaminergic neuron-specific responses. Neuroscience. 1994; 63:1021–1031. [PubMed: 7700507]

Kus L, Borys E, PIng Chu Y, Ferguson SM, Blakely RD, Emborg ME, Kordower JH, Levey AI, Mufson EJ. Distribution of high affinity choline transporter immunoreactivity in the primate central nervous system. J Comp Neurol. 2003; 463:341–357. [PubMed: 12820166]

Lança AJ, Adamson KL, Coen KM, Chow BL, Corrigall WA. The pedunculopontine tegmental nucleus and the role of cholinergic neurons in nicotine self-administration in the rat: a correlative neuroanatomical and behavioral study. Neuroscience. 2000; 96:735–742. [PubMed: 10727791]

Laviolette SR, van der Kooy D. The motivational valence of nicotine in the rat ventral tegmental area is switched from rewarding to aversive following blockade of the α7-subunit-containing nicotinic acetylcholine receptor. Psychopharmacology (Berl). 2003; 166:306–313. [PubMed: 12569428]

Lecomte MJ, De Gois S, Guerci A, Ravassard P, Faucon-Biguet N, Mallet J, Berrard S. Differential expression and regulation of the high-affinity choline transporter CHT1 and choline acetyltransferase in neurons of superior cervical ganglia. Mol Cell Neurosci. 2005; 28:303–313. [PubMed: 15691711]

Levey AI, Hallanger AE, Wainer BH. Choline acetyltransferase immunoreactivity in the rat thalamus. J Comp Neurol. 1987; 257:317–332. [PubMed: 3549798]

Lisman JE, Harris KM. Quantal analysis and synaptic anatomy - integrating two views of hippocampal plasticity. Trends Neurosci. 1993; 16:141–147. [PubMed: 7682347]

Littell, RC.; Nilliken, GA.; Stroup, WW.; Wolfinger, RD.; Schabenberger, O. Cary, NC: SAS Institute, Inc; 2006. SAS for Mixed Models.

Löffelholz, K.; Klein, J. Precursors: choline and glucose. In: Giacobini, E.; Pepeu, G., editors. The Brain Cholinergic System in Health and Disease. Boca Raton: Informa Healthcare; 2006. p. 75-84.

Losier BJ, Semba K. Dual projections of single cholinergic and aminergic brainstem neurons to the thalamus and basal forebrain in the rat. Brain Res. 1993; 604:41–52. [PubMed: 7681346]

Mathiisen, TM.; Nagelhus, EA.; Jouleh, B.; Torp, R.; Frydenlund, DS.; Mylonakou, M-N.; Amiry-Moghaddam, M.; Covolan, L.; Utvik, JK.; Riber, B.; Gujord, KM.; Knutsen, J.; Skare, Ø.; Laake, P.; Davanger, S.; Haug, F-M.; Rinvik, E.; Ottersen, OP. Postembedding immunogold cytochemistry of membrane molecules and amino acid transmitters in the central nervous system. In: Zaborszky, L.; Wouterlood, FG.; Lanciego, JL., editors. Neuroanatomical Tract-Tracing 3: Molecules, Neurons, and Systems. New York: Springer; 2005. p. 72-108.

Mike A, Castro NG, Albuquerque EX. Choline and acetylcholine have similar kinetic properties of activation and desensitization on the α7 nicotinic receptors in rat hippocampal neurons. Brain Res. 2000; 882:155–168. [PubMed: 11056195]

Misawa H, Nakata K, Matsuura J, Nagao M, Okuda T, Haga T. Distribution of the high-affinity choline transporter in the central nervous system of the rat. Neuroscience. 2001; 105:87–98. [PubMed: 11483303]

Murrin LC, Kuhar MJ. Activation of high-affinity choline uptake in vitro by depolarizing agents. Mol Pharmacol. 1976; 12:1082–1090. [PubMed: 1004491]

Nakata K, Okuda T, Misawa H. Ultrastructural localization of high-affinity choline transporter in the rat neuromuscular junction: enrichment on synaptic vesicles. Synapse. 2004; 53:53–56. [PubMed: 15150741]

Oakman SA, Faris PL, Cozzari C, Hartman BK. Characterization of the extent of pontomesencephalic cholinergic neurons' projections to the thalamus: comparison with projections to midbrain dopaminergic groups. Neuroscience. 1999; 94:529–547. [PubMed: 10579214]

Oakman SA, Faris PL, Kerr PE, Cozzari C, Hartman B. Distribution of pontomesencephalic cholinergic neurons projecting to substantia nigra differs significantly from those projecting to ventral tegmental area. J Neurosci. 1995; 15:5859–5869. [PubMed: 7666171]

Oda S, Kuroda M, Kakuta S, Tanihata S, Ishikawa Y, Kishi K. Ultrastructure of ascending cholinergic terminals in the anteroventral thalamic nucleus of the rat: a comparison with the mammillothalamic terminals. Brain Res Bull. 2003; 59:473–483. [PubMed: 12576145]

Okuda T, Haga T. High-affinity choline transporter. Neurochem Res. 2003; 28:483–488. [PubMed: 12675135]

Omelchenko N, Sesack SR. Laterodorsal tegmental projections to identified cell populations in the rat ventral tegmental area. J Comp Neurol. 2005; 483:217–235. [PubMed: 15678476]

Omelchenko N, Sesack SR. Cholinergic axons in the rat ventral tegmental area synapse preferentially onto mesoaccumbens dopamine neurons. J Comp Neurol. 2006; 494:863–875. [PubMed: 16385486]

Oshima S, Yamada K, Shirakawa T, Watanabe M. Changes of high-affinity choline transporter CHT1 mRNA expression during degeneration and regeneration of hypoglossal nerves in mice. Neurosci Lett. 2004; 365:97–101. [PubMed: 15245786]

Pan WX, Hyland BI. Pedunculopontine tegmental nucleus controls conditioned responses of midbrain dopamine neurons in behaving rats. J Neurosci. 2005; 25:4725–4732. [PubMed: 15888648]

Parent A, Paré D, Smith Y, Steriade M. Basal forebrain cholinergic and noncholinergic projections to the thalamus and brainstem in cats and monkeys. J Comp Neurol. 1988; 277:281–301. [PubMed: 2466060]

Parent M, Descarries L. Acetylcholine innervation of the adult rat thalamus: distribution and ultrastructural features in dorsolateral geniculate, parafascicular, and reticular thalamic nuclei. J Comp Neurol. 2008; 511:678–691. [PubMed: 18924144]

Parikh V, Apparsundaram S, Kozak R, Richards JB, Sarter M. Reduced expression and capacity of the striatal high-affinity choline transporter in hyperdopaminergic mice. Neuroscience. 2006; 141:379–389. [PubMed: 16675138]

Pidoplichko VI, Noguchi J, Areola OO, Liang Y, Peterson J, Zhang T, Dani JA. Nicotinic cholinergic synaptic mechanisms in the ventral tegmental area contribute to nicotine addiction. Learn Mem. 2004; 11:60–69. [PubMed: 14747518]

Pierce JP, Lewin GR. An ultrastructural size principle. Neuroscience. 1994; 58:441–446. [PubMed: 8170532]

Rasmussen BA, Perry DC. An autoradiographic analysis of [^{125}I]α-bungarotoxin binding in rat brain after chronic nicotine exposure. Neurosci Lett. 2006; 404:9–14. [PubMed: 16750882]

Redgrave P, Gurney K, Reynolds J. What is reinforced by phasic dopamine signals? Brain Res Rev. 2008; 58:322–339. [PubMed: 18055018]

Ribeiro FM, Alves-Silva J, Volknandt W, Martins-Silva C, Mahmud H, Wilhelm A, Gomez MV, Rylett RJ, Ferguson SS, Prado VF, Prado MA. The hemicholinium-3 sensitive high affinity choline transporter is internalized by clathrin-mediated endocytosis and is present in endosomes and synaptic vesicles. J Neurochem. 2003; 87:136–146. [PubMed: 12969261]

Roskoski R Jr. Acceleration of choline uptake after depolarization-induced acetylcholine release in rat cortical synaptosomes. J Neurochem. 1978; 30:1357–1361. [PubMed: 670977]

Satoh K, Fibiger HC. Cholinergic neurons of the laterodorsal tegmental nucleus: efferent and afferent connections. J Comp Neurol. 1986; 253:277–302. [PubMed: 2432101]

Schilström B, Fagerquist MV, Zhang X, Hertel P, Panagis G, Nomikos GG, Svensson TH. Putative role of presynaptic α7* nicotinic receptors in nicotine stimulated increases of extracellular levels of glutamate and aspartate in the ventral tegmental area. Synapse. 2000; 38:375–383. [PubMed: 11044884]

Schultz W. Behavioral dopamine signals. Trends Neurosci. 2007; 30:203–210. [PubMed: 17400301]

Semba K, Reiner PB, Fibiger HC. Single cholinergic mesopontine tegmental neurons project to both the pontine reticular formation and the thalamus in the rat. Neuroscience. 1990; 38:643–654. [PubMed: 2176719]

Shibata H. Topographic organization of subcortical projections to the anterior thalamic nuclei in the rat. J Comp Neurol. 1992; 323:117–127. [PubMed: 1385491]

Sikes RW, Vogt BA. Afferent connections of anterior thalamus in rats: sources and association with muscarinic acetylcholine receptors. J Comp Neurol. 1987; 256:538–551. [PubMed: 3558887]

Simon H, Le Moal M, Calas A. Efferents and afferents of the ventral tegmental A10 region studied after local injection of [^{3}H] leucine and horseradish peroxidase. Brain Res. 1979; 178:17–40. [PubMed: 91413]

Simon JR, Atweh S, Kuhar MJ. Sodium-dependent high affinity choline uptake: a regulatory step in the synthesis of acetylcholine. J Neurochem. 1976; 26:909–922. [PubMed: 1271069]

Simon JR, Kuhar MJ. Impulse-flow regulation of high affinity-choline uptake in brain cholinergic terminals. Nature. 1975; 255:162–163. [PubMed: 165430]

Slotkin TA, Nemeroff CB, Bisette G, Seidler FJ. Overexpression of the high affinity choline transporter in cortical regions affected by Alzheimer's disease. Evidence from rapid autopsy studies. J Clin Invest. 1994; 94:696–702. [PubMed: 8040324]

Slotkin TA, Seidler FJ, Crain BJ, Bell JM, Bisette G, Nemeroff CB. Regulatory changes in presynaptic cholinergic function assessed in rapid autopsy material from patients with Alzheimer disease: implications for etiology and therapy. Proc Natl Acad Sci USA. 1990; 87:2452–2455. [PubMed: 2320567]

Small, SV. Measurement of section thickness. Bocciarelli, DS., editor. Tipografia, Poliglotta Vaticana, Rome: 1968. p. 609-610.

Sofroniew MV, Priestley JV, Consolzaione A, Eckenstein F, Cuello AC. Cholinergic projections from the midbrain and pons to the thalamus in the rat, identified by combined retrograde tracing and choline acetyltransferase immunohistochemistry. Brain Res. 1985; 329:213–223. [PubMed: 3978443]

Sparenborg S, Gabriel M. Local norepinephrine depletion and learning-related neuronal activity in cingulate cortex and anterior thalamus of rabbits. Exp Brain Res. 1992; 92:267–285. [PubMed: 1493864]

Standaert DG, Saper CB, Rye DR, Wainer BH. Colocaliztion of atriopeptin-like immunoreactivity with choline acetyltransferase and substance P-like immunoreactivity in the pedunculopontine and laterodorsal tegmental nuclei in the rat. Brain Res. 1986; 382:163–168. [PubMed: 2429724]

Stanton TL, Johnson GV. In vitro measurements of cholinergic activity in brain regions of hibernating ground squirrels. Brain Res Bull. 1987; 18:663–667. [PubMed: 3607532]

Sutin EL, Jacobowitz DM. Localization of substance P mRNA in cholinergic cells of the rat laterodorsal tegmental nucleus: *in situ* hybridization histochemistry and immunocytochemistry. Cell Mol Neurobiol. 1990; 10:19–31. [PubMed: 1692261]

Takashina K, Bessho T, Mori R, Eguchi J, Saito K. MKC-231, a choline uptake enhancer: (2) Effect on synthesis and release of acetylcholine in AF64A-treated rats. J Neural Transm. 2008; 115:1027–1035. [PubMed: 18446264]

Tomimoto H, Kamo H, Kamyama M, McGeer PL, Kimura H. Descending projections of the basal forebrain in the rat demonstrated by the anterograde neural tracer *Phaseolus vulgaris* leucoagglutinin (PHA-L). Brain Res. 1987; 425:248–255. [PubMed: 2827844]

Umbriaco D, Watkins KC, Descarries L, Cozzari C, Hartman BK. Ultrastructural and morphometric features of the acetylcholine innervation in adult rat parietal cortex: an electron microscopic study in serial sections. J Comp Neurol. 1994; 348:351–373. [PubMed: 7844253]

Uteshev VV, Meyer EM, Papke RL. Regulation of neuronal function by choline and 4OH-GTS-21 through α7 nicotinic receptors. J Neurophysiol. 2003; 89:1797–1806. [PubMed: 12611953]

Veznedaroglu E, Milner TA. Elimination of artifactual labeling of hippocampal mossy fibers seen following pre-embedding immunogold-silver technique by pretreatment with zinc chelator. Microsc Res Tech. 1992; 23:100–101. [PubMed: 1327296]

Vincent SR, Satoh K, Armstrong DM, Fibiger HC. Substance P in the ascending cholinergic reticular system. Nature. 1983; 306:688–691. [PubMed: 6197654]

Vogelsberg V, Neff NH, Hadjiconstatntinou M. Cyclic AMP-mediated enhancement of high-affinity choline transport and acetylcholine synthesis in brain. J Neurochem. 1997; 68:1062–1070. [PubMed: 9048751]

Vogt LJ, Vogt BA, Sikes RW. Limbic thalamus in rabbit: architecture, projections to cingulate cortex and distribution of muscarinic acetylcholine, GABAA, and opioid receptors. J Comp Neurol. 1992; 319:205–217. [PubMed: 1326004]

Warburton EC, Aggleton JP. Differential deficits in the Morris water maze following cytotoxic lesions of the anterior thalamus and fornix transection. Behav Brain Res. 1999; 98:27–38. [PubMed: 10210519]

Wecker L, Dettbarn WD. Relationship between choline availability and acetylcholine synthesis in discrete regions of rat brain. J Neurochem. 1979; 32:961–967. [PubMed: 430073]

Woolf NJ, Gould E, Butcher LL. Nerve growth factor receptor is associated with cholinergic neurons of the basal forebrain but not the pontomesencephalon. Neuroscience. 1989; 30:143–152. [PubMed: 2546097]

Yamamura HI, Snyder SH. Choline: high-affinity uptake by rat brain synaptosomes. Science. 1972; 178:626–628. [PubMed: 5086398]

Yamamura HI, Snyder SH. High affinity transport of choline into synaptosomes of rat brain. J Neurochem. 1973; 21:1355–1374. [PubMed: 4771436]

Yan Q, Johnson EM Jr. Immunohistochemical localization and biochemical characterization of nerve growth factor receptor in adult rat brain. J Comp Neurol. 1989; 290:585–598. [PubMed: 2559110]

Yeomans JS. Role of tegmental cholinergic neurons in dopaminergic activation, antimuscarinic psychosis and schizophrenia. Neuropsychopharmacology. 1995; 12:3–16. [PubMed: 7766284]

Yeomans JS, Mathur A, Tampakeras M. Rewarding brain stimulation: role of the tegmental cholinergic neurons that activate dopamine neurons. Behav Neurosci. 1993; 107:1077–1087. [PubMed: 8136061]

Zapata A, Capdevila JL, Trullas R. Role of high-affinity choline uptake on extracellular choline and acetylcholine evoked by NMDA. Synapse. 2000; 35:272–280. [PubMed: 10657037]

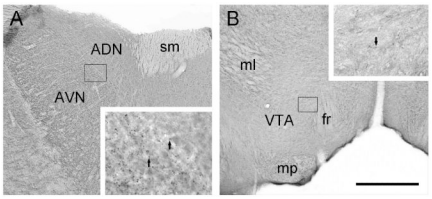

Figure 1.

Light micrographic images of coronal sections through the rat AVN (**A**) and VTA (**B**) illustrating immunoperoxidase labeling for CHT. In **A**, immunoreactivity for CHT appears to be denser in the AVN than in the anterodorsal thalamic nucleus (ADN). The boxed region shown at higher magnification in the insert straddles the two divisions and illustrates immunolabeled puncta (arrows) representing probable axon varicosities. Note the absence of these puncta in the adjacent ADN. **B** shows relatively uniform CHT staining in the VTA. The boxed region shown at higher magnification in the insert illustrates immunoreactive puncta (arrow) that appear at lower density than in the AVN. Abbreviations: fr, fasciculus retroflexus; ml, medial lemniscus; mp, mammillary peduncle; sm, stria medularis. Scale bar represents 500 μm in A and B, 100 μm in inserts.

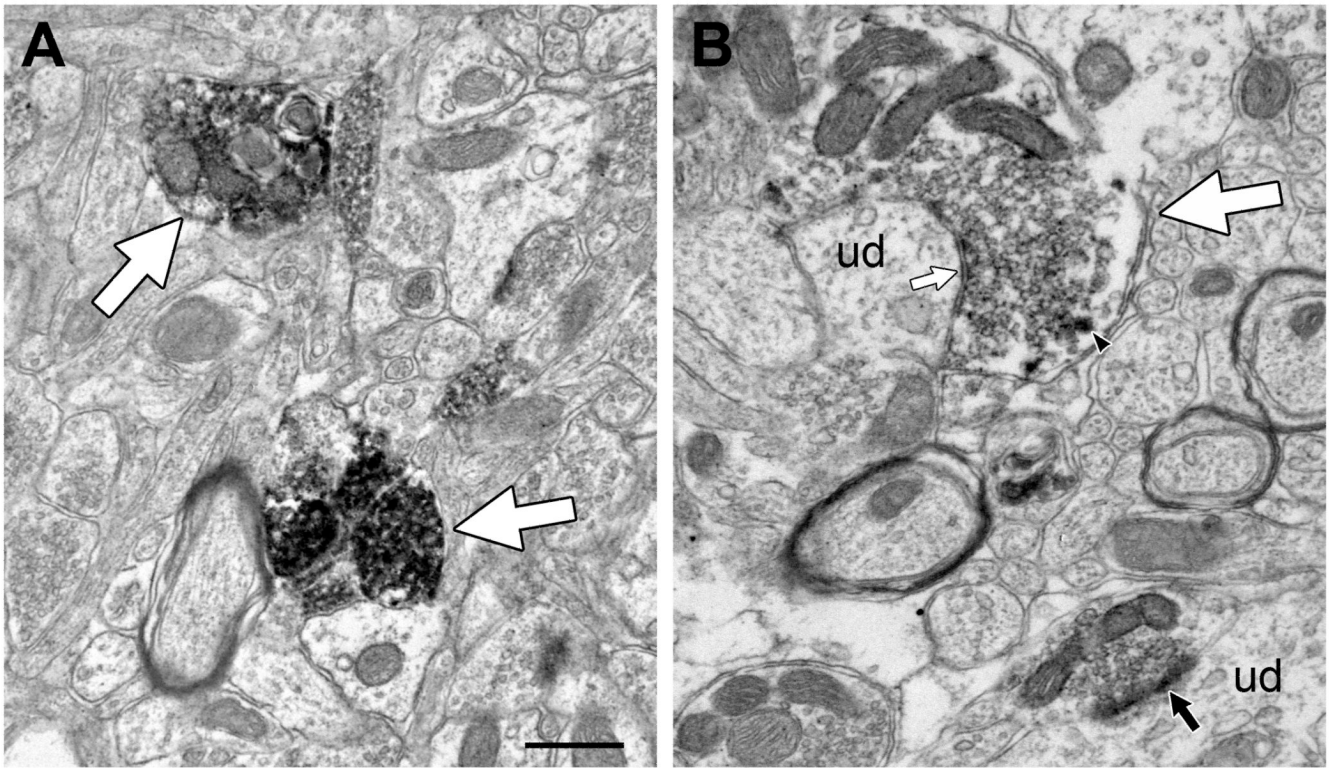

Figure 2.

Electron micrographs showing representative immunoperoxidase labeling for CHT in axonal profiles (large white arrows) in the AVN (**A**) and VTA (**B**). The reaction product typically appears to be denser in labeled AVN profiles than those observed in the VTA, although a range of immunoreactive densities is evident. CHT positive profiles also appear to be more numerous in the AVN than in the VTA, consistent with the observations made at the light microscopic level. The lightly labeled CHT varicosities in the VTA form symmetric (small white arrow) or asymmetric (black arrow) synapses onto unlabeled dendrites (ud). One of these also contains a dense-cored vesicle (arrowhead). The heavy peroxidase reaction product in AVN profiles makes it difficult to identify dense-core vesicles in this region. Scale bar represents 0.5 μm.

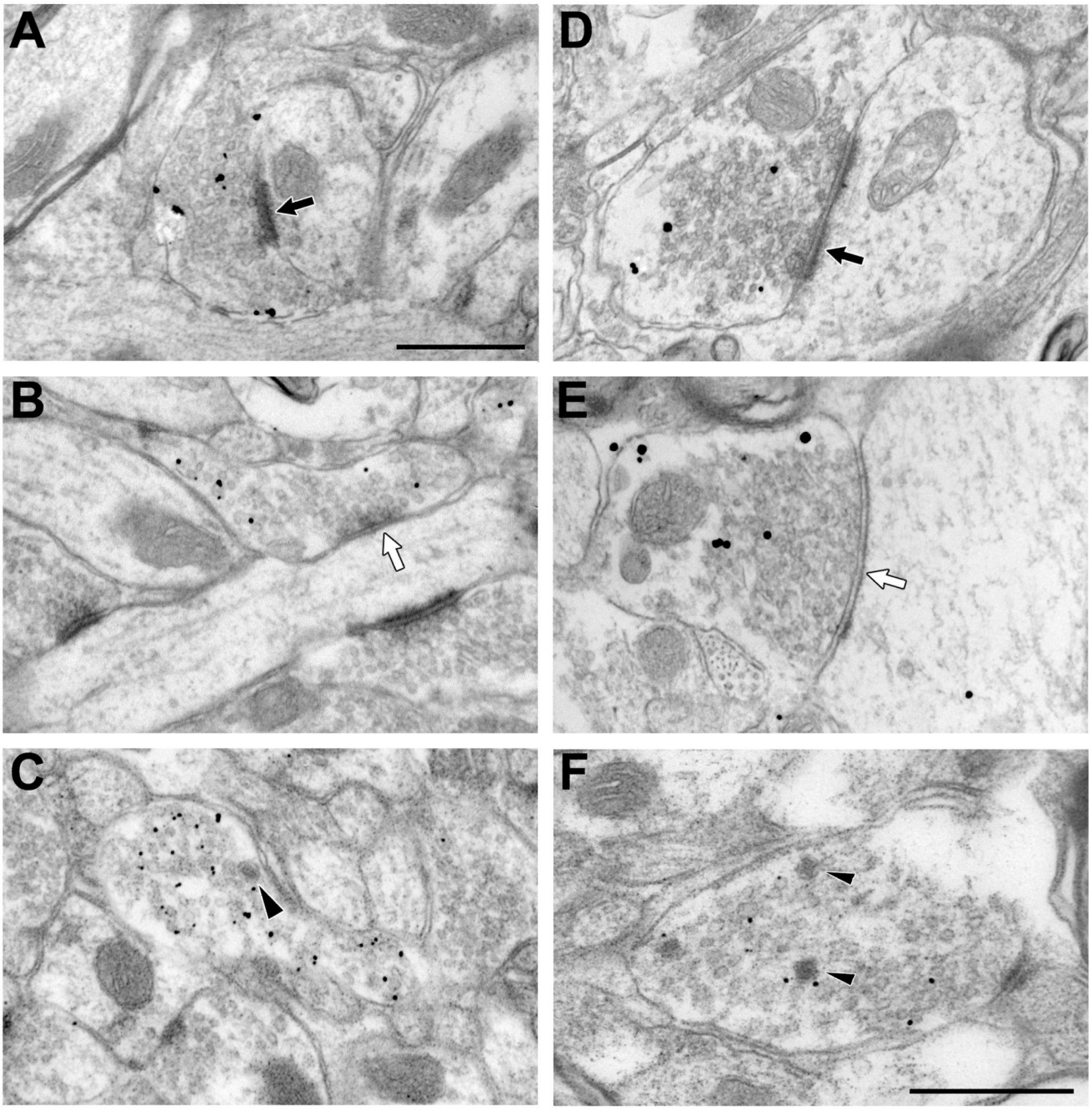

Figure 3.
Electron micrographs showing the morphological features of CHT-positive profiles in the AVN (**A–C**) and VTA (**D–F**). CHT labeled profiles form both asymmetric (black arrows, **A & D**) and symmetric (white arrows; **B & E**) types of synaptic contacts with unlabeled dendrites in the regions examined. Occasionally, dense-cored vesicles are observed in labeled profiles (arrowheads in **C & F**). Scale bar represents 0.5 μm.

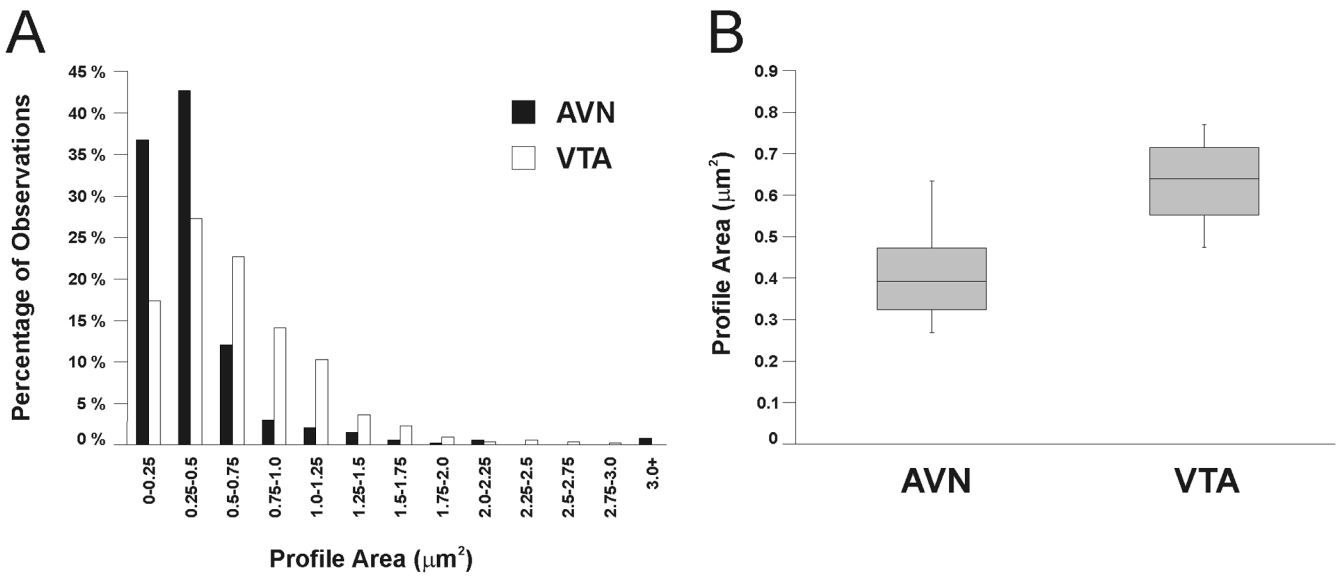

Figure 4.

Frequency distribution (**A**) and quartile plots (**B**) of CHT-labeled axon profile areas observed in the AVN and VTA. **A**: Histogram illustrating the frequency of areas measured for profiles immunoreactive for CHT in the rat AVN (black bars) or VTA (white bars). Each bar represents the percentage of the total sample of immunoreactive profiles having a particular area. **B**: Box plots illustrating the range of mean profile areas (between whiskers) as well as the median values (central line) and the middle 50% of values observed in each region (shaded boxes). Mean profile areas were computed by averaging profile areas within each region for each rat.

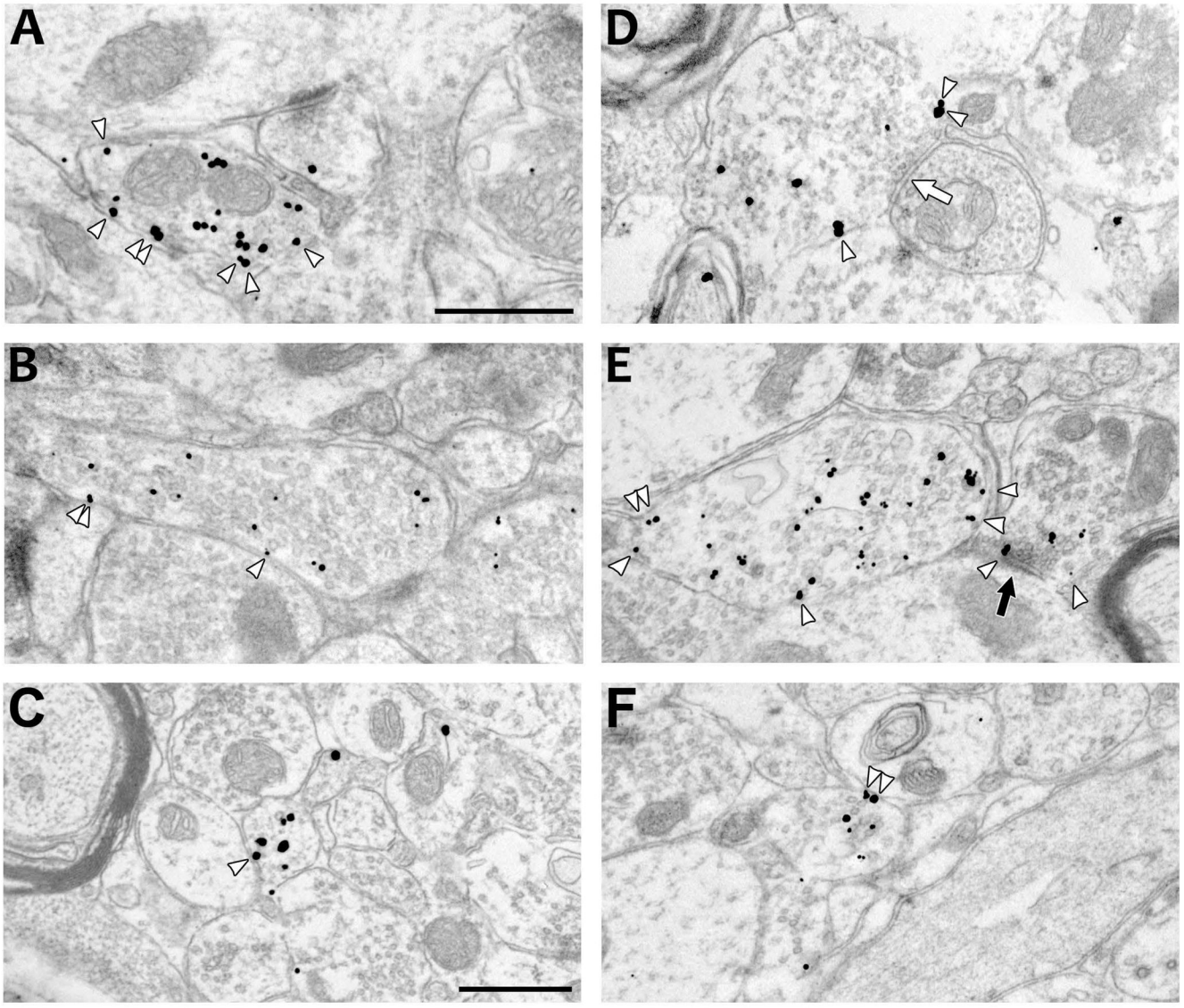

Figure 5.

Electron micrographs illustrating CHT positive-profiles labeled by immunogold-silver in the AVN (**A–C**) and VTA (**D–F**) and displaying a range of sizes and also total gold and membrane gold densities. Arrowheads indicate gold-silver particles counted as being in association with the plasma membrane. Occasional symmetric (white arrow in **D**) or asymmetric (black arrow in **E**) synapses onto dendrites are exhibited by CHT-immunoreactive axons. Scale bars represent 0.5 μm. Scale bar in **A** represents 0.5 μm in **A** and **B**; scale bar in **C** represents 0.5 μm in **C–F**.

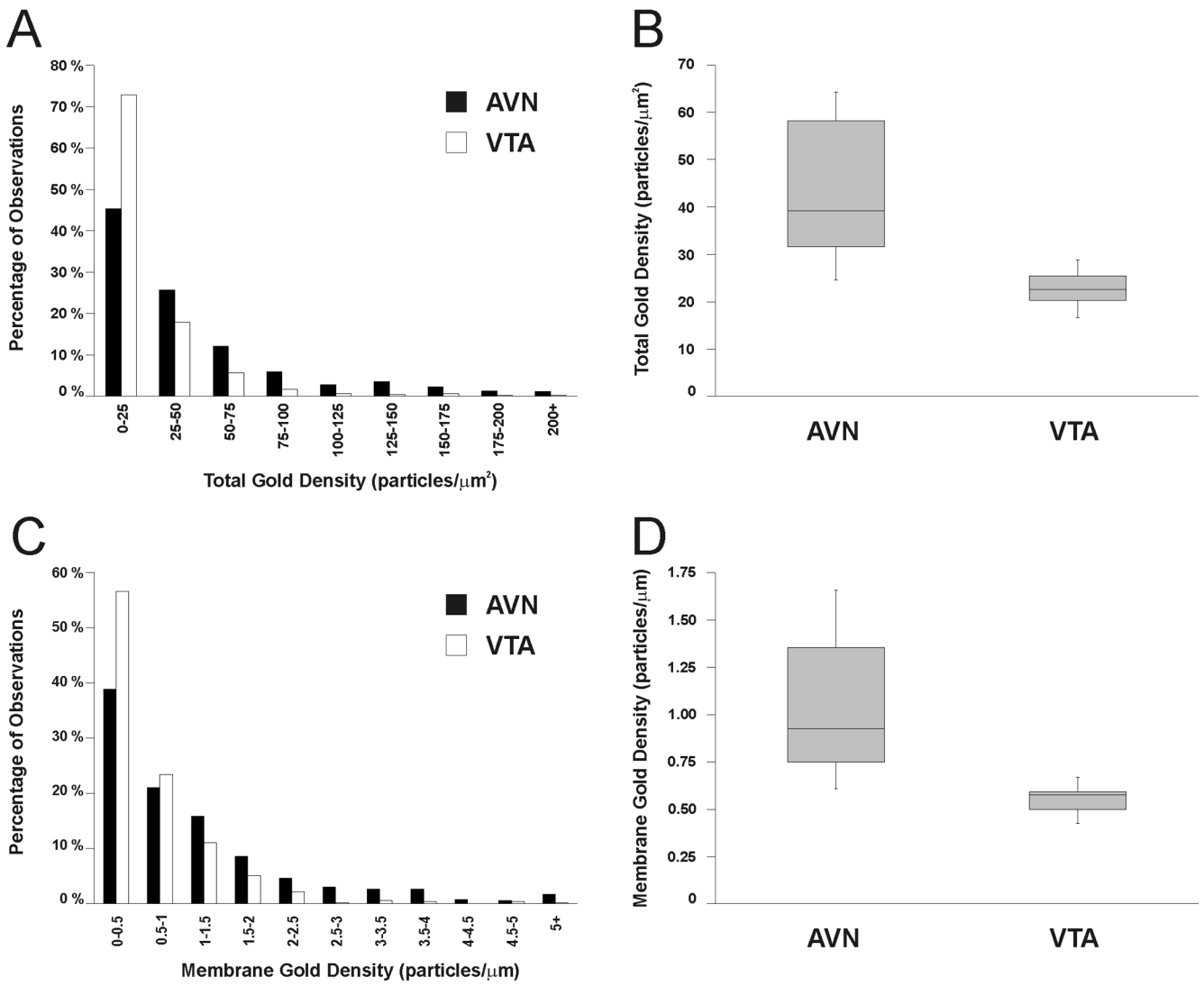

Figure 6.

Frequency distributions (**A&C**) and quartile plots (**B&D**) of values observed for the total gold density (# gold particles/profile area; **A&B**) and membrane gold density (# membrane associate gold particles/profile perimeter; **C&D**) in the sample of CHT-labeled axonal profiles in the AVN and VTA. **A&C**: Histograms illustrating the frequency of total gold density (**A**) or membrane gold density (**C**) measured for profiles immunoreactive for CHT in the rat AVN (black bars) or VTA (white bars). Each bar represents the percentage of the total sample of immunoreactive profiles having a particular density. **B&D**: Box plots illustrating the range of mean total gold density and mean membrane gold density (between whiskers in **B** and **D**, respectively) as well as the median values (central lines) and the middle 50% of values observed in each region (shaded boxes). Mean total gold density and mean membrane gold density were computed by averaging total gold density and membrane gold density, respectively, within each region for each rat.

Table 1

Sampling Scheme for Ultrastructural Analysis

		Number of profiles analyzed		
Animal	**Region**	**Data set 1 serial sections**	**Data set 2 single sections**	**Data set 3 all profiles**
1	AVN	30	68	98
	VTA	26	65	91
2	AVN	7	93	100
	VTA	0	93	93
3	AVN	89	0	89
	VTA	107	0	107
4	AVN	48	44	92
	VTA	39	47	86
5	AVN	80	0	80
	VTA	56	0	56
6	AVN	79	0	79
	VTA	76	0	76
Total		637	410	1047